Available online at www.sciencedirect.com
ScienceDirect
Carbon 45 (2007) 416–423
CARBON
www.elsevier.com/locate/carbon

Structural and mechanical characterization of platelet graphite nanofibers

Xinqi Chen [a], Zhi-Hui Xu [b], Xiaodong Li [b], Medhat A Shaibat [c], Yoshitaka Ishii [c], Rodney S. Ruoff [d,*]

[a] NUANCE Center, Northwestern University, Evanston, IL 60208, USA
[b] Department of Mechanical Engineering, University of South Carolina, Columbia, SC 29208, USA
[c] Department of Chemistry, University of Illinois at Chicago, Chicago, IL 60607, USA
[d] Department of Mechanical Engineering, Northwestern University, Evanston, IL 60208, USA

Received 12 June 2006; accepted 30 August 2006
Available online 1 November 2006

Abstract

Platelet graphite nanofibers have been characterized by scanning electron microscopy, transmission electron microscopy, electron diffraction, X-ray photoemission spectroscopy, and atomic force microscopy. The results show that the graphene sheets are stacked parallel to each other and are perpendicular to the fiber axis; the interlayer spacing is 0.34 nm. A small fraction of carbon atoms are bonded to oxygen. Solid-state nuclear magnetic resonance shows that hydrogenated carbons are under the detection limit (<5%) and that the nanofibers are dominated by sp^2-bonded carbons. Mechanical measurements were made on individual nanofibers by nanoindentation.

1. Introduction

Graphite nanofiber (GNF) material is produced by the decomposition of carbon-containing gases over metal catalyst particles at temperatures ranging from 400 to 800 °C. The structures consist of graphene sheets arranged parallel, perpendicular or at a skewed orientation with respect to the long axis of the fiber [1,2]. This material is also called ''platelet graphite nanofiber''. These structures contain a large number of edges, which in turn constitute sites readily available for chemical or physical interaction, particularly adsorption. Such structures may have possibilities for hydrogen storage, for example if the interlayer separation could be altered by appropriate pillars. Due to the outstanding electrical and mechanical properties of graphite platelets, platelet GNF might find use as a filler for composites.

The study on the structure and the mechanical properties of platelet GNF is far from complete. In this paper, we discuss the structure as determined by scanning electron microscopy (SEM), transmission electron microscopy (TEM), X-ray photoemission spectroscopy (XPS), and solid-state nuclear magnetic resonance (SSNMR). We also present nanoindentation measurements on individual platelet GNF and discuss their meaning.

2. Experimental methods

Platelet GNF was purchased from Catalytic Materials LLC (Holliston, MA). It was synthesized from the catalytic decomposition of CO/H_2 mixtures over powdered Fe–Cu catalysts at temperatures around 600 °C.[1] The powder sample was dispersed in ethanol and a few droplets of the suspension were put on a piece of silicon wafer for SEM (Leo1525 FEG SEM) and nanoindentation measurements. One droplet of this suspension was put on a lacey carbon TEM grid (Ted Pella, Inc.) for TEM analysis (Hitachi HF2000). The selected area electron diffraction was performed on a

* Corresponding author. Fax: +1 847 491 3915.
E-mail address: r-ruoff@northwestern.edu (R.S. Ruoff).

[1] The GNF's studied here were evidently made by the same method as described in references [1,2]; private communication with Dr. R.T.K. Baker.

0008-6223/$ - see front matter © 2006 Elsevier Ltd. All rights reserved.
doi:10.1016/j.carbon.2006.08.025

Hitachi 8100 TEM. XPS analysis was performed with an Omicron ESCA probe, which was equipped with an EA125 energy analyzer. Photoemission was stimulated by monochromatic Al K radiation (1486.6 eV) with an operating power of 300 W. The elemental analysis of the as-received material was performed by Atlantic Microlab, Inc. for C, H, O, S, Cl, and N (sample dried in vacuum at 150 °C for 2 h).

The as-received powder sample was used for SSNMR measurement without further treatment of any kind. All the SSNMR spectra were recorded at a ^{1}H frequency of 400.2 MHz (9.4 T) with a Varian Infinity-plus SSNMR spectrometer (Palo Alto, CA) using a home-built 2.5 mm double-resonance MAS probe, which provides stable spinning up to 30 kHz. To minimize contribution of background ^{13}C signals, the standard Torlon spacer in the MAS rotor was replaced by NaCl and the end-cap of the rotor was shortened by ~3 mm. Residual background signals were removed by subtracting the spectra obtained without the sample. ^{1}H RF decoupling was not employed so as to minimize the background signals from the outside of the rotor; line broadening due to ^{13}C–^{1}H dipolar couplings are minimized by fast spinning at 20 kHz [3]. To avoid baseline distortion, a rotor-synchronous echo sequence (τ_R–π–τ_R) was applied prior to signal acquisition, where τ_R denotes one rotor cycle. All the experiments were performed with a Varian variable temperature (VT) controller and a VT stack, which maintained VT cooling air at −5 °C and the sample temperature under fast spinning approximately at 20 °C. In all experiments, the π- and $\pi/2$-pulse widths for ^{13}C were 5.6 μs and 2.8 μs, respectively, while the π-pulse width for ^{1}H was 6.0 μs. Since loading this sample changed the probe Q-factor considerably, the pulse widths were calibrated with standard samples mixed with the GNF sample. All the data were processed with Varian Spinsight software. To obtain higher sensitivity, we tried to perform the experiments with a Bruker double-resonance 5-mm MAS probe, which accommodates a larger sample amount. However, the sample seems to have an unusual dielectric constant compared with those of typical organic samples; the commercial NMR probe could not be tuned with the sample. Resonance positions were referenced with respect to tetramethylsilane (TMS) using the CH_2 resonance of adamantane at 38.56 ppm as a secondary reference.

Platelet GNFs were spread on a silicon wafer substrate and observed using a tapping mode atomic force microscope (AFM; NanoScope Dimension™ 3100, Digital Instruments, Veeco Metrology Group, Woodbury, New York). The silicon wafer with an elastic modulus of 165 GPa and a hardness of 12 GPa [4] was chosen as the substrate because of its extremely flat surface, which provides good contact for the platelet GNFs. Nanoindentation fracture tests were performed on the platelet GNFs using a special diamond-tipped cantilever, which has an included angle about 60° and a tip radius less than 50 nm. The sharp diamond-tipped cantilever of AFM results in fracture of the GNF, which can be used to estimate the fracture energy. To avoid the fracture of the GNFs so that the mechanical properties of the GNFs can be accurately determined, nanoindentation tests were carried out with a Triboscope (Hysitron, Inc.) using a relatively blunt pyramidal Berkovich indenter, which has an included angle of 142.35° and a tip radius of 100 nm. During indentation, a peak force of 24 μN was first applied in 2.5 s and then totally released in the same time. This force produces an indent normally shallower than 10 nm, which is much smaller than the dimension (over 100 nm) of the GNF and therefore reduces the possible substrate or size effect on the measurement of the mechanical properties [5].

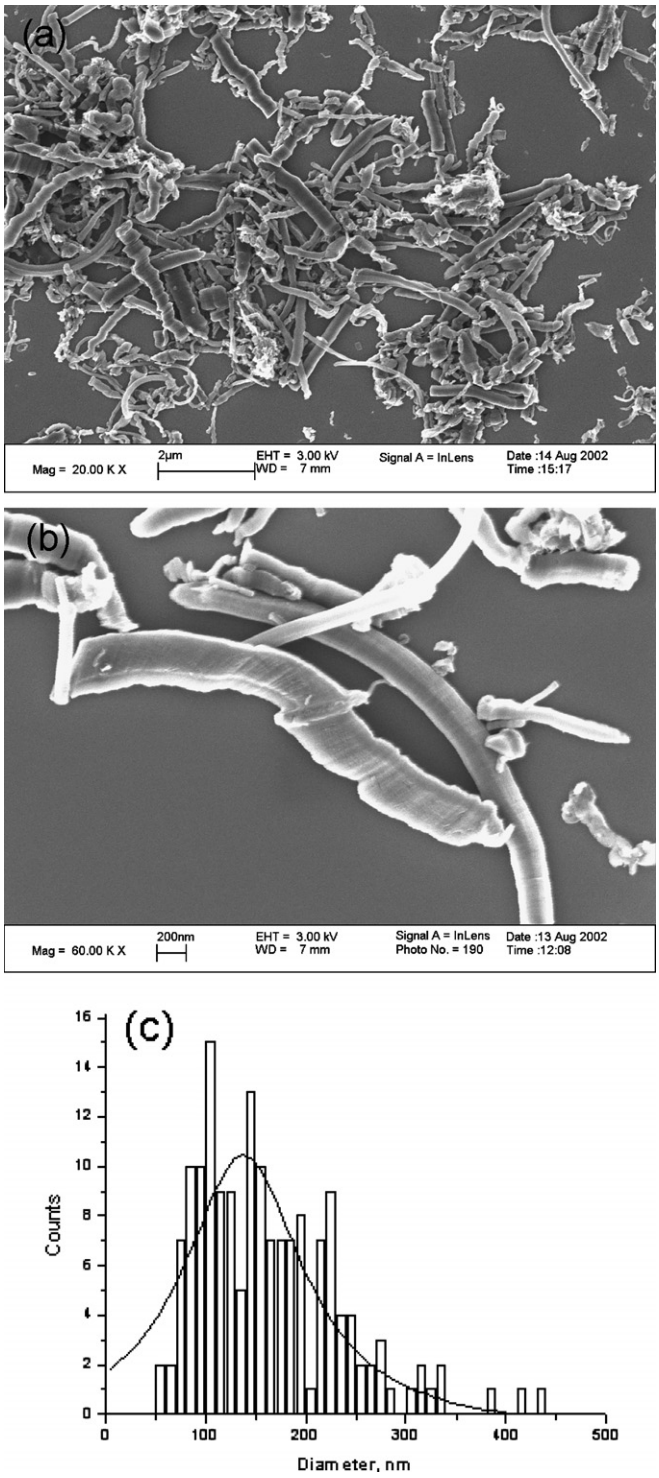

Fig. 1. (a) Low-mag and (b) high-mag SEM images of platelet graphite nanofibers. (c) Histogram of the fiber diameter distribution.

3. Results and discussion

3.1. SEM, TEM, and XPS characterization

Fig. 1(a) and (b) shows low-mag and high-mag SEM images of platelet GNFs. There are curved and straight nanofibers present in the primary sample. Fig. 1(c) shows the histogram of the diameter distribution. The solid line is a Lorentzian fit and the center of the peak is 138 nm. The 'diameter' of the nanofibers is in the range of a few tens to a few hundreds of nanometers and the lengths vary from sub-micrometer to a few micrometers. TEM images are shown in Fig. 2. The graphene sheets are stacked parallel and oriented perpendicular to the long axis of the fiber. They are curved at the edges, however there is no folding observed in the high-resolution TEM image. The

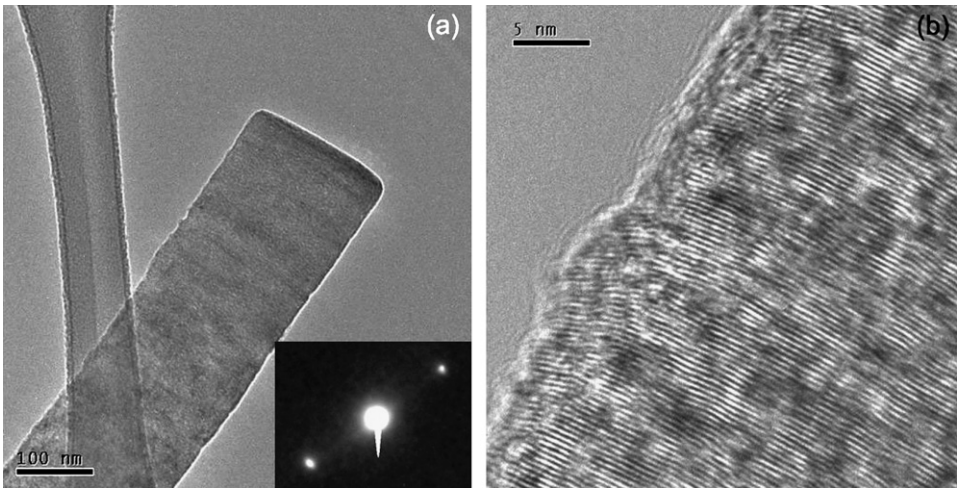

Fig. 2. TEM image of graphite nanofibers: (a) low-mag TEM image and (b) high-mag TEM image. Inset of (a) is the selected area electron diffraction of the GNF.

selected area electron diffraction pattern is shown in the inset of the TEM image in Fig. 2(a) and the spacing between the layers (believed to be finite-sized graphene sheets) is ~0.34 nm, thus similar to graphite. The XPS spectrum of GNFs indicates the presence of just carbon and oxygen. C 1s XPS spectrum (shown in Fig. 3) could be deconvoluted to five components that correspond to carbon atoms in different chemical bonding configurations: the non-oxygenated ring C at a binding energy of 284.9 eV, β-shifted C (due to their juxtaposition to O–C=O groups) at 285.9 eV, C in C–O bonds at 287.6 eV, C in O–C=O groups at 289.2 eV, and a π-π* 'shake-up satellite' at 291 eV [6,7]. Quantitative analysis of the C 1s and O 1s XPS peak intensities indicates a higher level of oxygen than is obtained by elemental analysis of the bulk material. The four XPS measurements give an O:C atomic ratio of $2.6\% \pm 1\%$ while elemental analysis of bulk materials provides an O:C atomic ratio of $0.4\% \pm 0.3\%$. Since XPS is a surface-sensitive analytical technique, the disagreement could arise from a higher degree of oxygenation of the surface of these materials and/or surface adsorption of various contaminants. Elemental analysis also indicates a H:C atomic ratio of 3.7%. The Cl:C atomic ratio is less than 0.09% and there is no sulfur or nitrogen at the limits of detection of elemental analysis (0.3 weight%). An acid treatment has been used to remove the catalyst metals used for the synthesis of the GNF's,[2] thus our interest in probing for the possible presence of S or N from acid treatment.

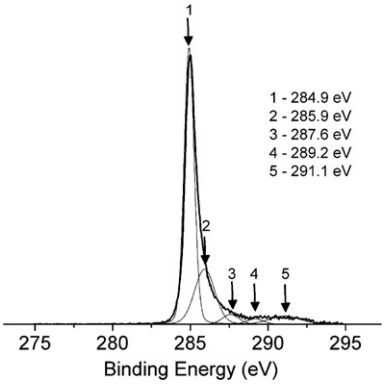

Fig. 3. C 1s XPS spectrum of graphite nanofibers.

3.2. Solid-state NMR characterization

Fig. 4 shows a ^{13}C Magic Angle Spinning (MAS) spectrum obtained for 14.4 mg of platelet GNF with single π/2-pulse excitation. The spectrum displays one broad peak centered around 80 ppm. We assigned this peak to sp^2 carbons based on the chemical shift. This 80 ppm resonance is shifted to lower frequency, compared with that of typical sp^2 carbons located at 110–160 ppm [8]. The ^{13}C isotropic chemical shifts (δ_{iso}) of graphite are reported to be ~120 ppm with principal values of $\delta_{\|}$ at 0 ppm and $\delta_{\perp}$ at 180 ppm [9], where $\delta_{iso} = (\delta_{\|} + 2\delta_{\perp})/3$, and $\delta_{\|}$ and $\delta_{\perp}$ denote anisotropic shifts when a static field is applied parallel and perpendicular to the *c*-axis of the graphite crystal, respectively. However, Hiroyama and Kume reported that for highly oriented pyrolytic graphite (HOPG) $\delta_{\|}$ shows a temperature-dependent large shielding, which is about −300 ppm at room temperature while $\delta_{\perp}$ is constant at 180 ppm between 77 and 473 K [10]; thus $\delta_{iso} \sim 20$ ppm for HOPG. From the temperature dependence of the anisotropic magnetic susceptibility of this sample, this unusual shift of $\delta_{\|}$ was explained as a shift originating from π-π* band interactions [10] or local fields due to "extended ring current" effects from stacked graphene sheets [11]. Similar effects were observed for graphite-like carbon materials obtained by a heat treatment of coconut endocarp above 2000 °C, for which δ_{iso} of ~90 ppm was reported [12]. Since

[2] Private communication with Dr. R.T.K. Baker who provided this material.

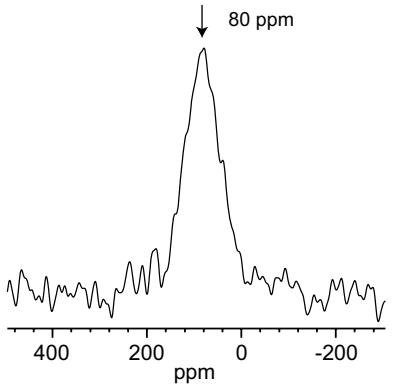

Fig. 4. A ^{13}C MAS spectrum of platelet graphite nanofibers (14.4 mg) obtained at ^{13}C frequency of 100.6 MHz with a single $\pi/2$-pulse excitation. The spectrum was acquired at a spinning speed of 20,000 Hz ± 5.0 Hz without ^{1}H RF decoupling and with recycle delays of 19.5 s. Background signals were removed by subtracting the spectrum obtained without the sample. The experimental time was 10 h for 1840 scans for each spectrum with or without the sample. Gaussian broadening of 10 ppm was applied to the spectrum.

the present sample displayed SEM and TEM images suggesting well-ordered stacked graphene sheet structures, it is highly likely that the low frequency shift of the 80 ppm resonance for sp^2-bonded carbons in the GNF sample arises from magnetic and/or electronic interactions associated with stacked sheet structures.

The amount of carbon in the platelet GNF sample estimated from the ^{13}C SSNMR spectrum in Fig. 4 was 0.51 mmol, based on comparison with a ^{13}C MAS spectrum of the CH_3 group of L-alanine (11.9 mg) obtained in the same way as that for platelet GNF, except for shorter recycle delays (0.5 s), which reflect a shorter longitudinal spin relaxation time (T_1) of the $^{13}CH_3$ group. The recycle delay for the ^{13}C MAS spectrum of the GNF in Fig. 4 is 19.5 s. The effects of the recycle delays shorter than $3T_1$ (39 s) and signal decay during the echo periods were included in the above calculation. This quantity of carbon is 43% of the 14.4 mg weight (1.20 mmol; assuming that the GNF sample is composed purely of C). One reason that we did not observe the total number of carbons in the sample might be due to a long T_1 for some missing carbon species. If ^{13}C T_1 is much longer than 19.5 s, the ^{13}C signals are not observable. The ^{13}C T_1 value for the observed signals was found to be 13 s for the overall spectrum range.

The line width of the peak at 80 ppm is broad (~90 ppm). Our transverse relaxation time (T_2) measurement using a spin echo sequence confirmed that homogeneous broadening accounts for only 4 ppm of the line width, so the width is primarily due to heterogeneous broadening. Possible sources of the line broadening include bulk magnetic susceptibility shifts, homogeneous and heterogeneous broadening due to paramagnetic impurities or radicals, and structural heterogeneity including modes of sheet stacking, which could modulate chemical and Knight shifts. The large line width of the ^{13}C peak may be also due to the presence of different chemical species. Pan et al. discussed sp^3-type carbons having a ^{13}C chemical shift around 40 ppm as well as sp^2-type carbons having ^{13}C shifts at 130 ppm for an amorphous carbon sample that was prepared by rf sputtering of pure graphite in a high vacuum system [13]. Although we think that the signal at 80 ppm is mostly due to sp^2-bonded carbon, it is possible that some sp^3 carbons contribute to a small shoulder peak around 40 ppm. The sp^3-bonded C atoms in carbon materials typically contain more protonated carbons than sp^2 groups [14,15]. Thus, we attempted to evaluate the possible presence of protonated carbons by ^{13}C SSNMR in order to identify sp^3-bonded carbons.

To estimate the amount of protonated ^{13}C in the GNF sample, we performed a ^{13}C–^{1}H dipolar dephasing experiment using a ^{13}C–^{1}H REDOR sequence [3,16]. Fig. 5 shows ^{13}C MAS spectra obtained (a) without, and (b) with ^{13}C–^{1}H dipolar dephasing, together with the difference spectrum between (a) and (b) shown in Fig. 5(c). This experiment with ^{13}C–^{1}H dephasing is designed to selectively remove signals of protonated ^{13}C. The ^{13}C–^{1}H REDOR sequence removes most of the ^{13}C signals (~90%) for ^{13}CH and $^{13}CH_2$ in rigid systems, while for CH_3 (due to methyl rotation), the REDOR sequence typically removes ~ 50% of the signals because of methyl rotation [3]. Assuming the system is rigid, we attempted to determine the amount of protonated sp^2 and sp^3-bonded carbons from the difference spectrum in Fig. 5(c), which is attributed to the signals of protonated ^{13}C groups. Since the difference spectrum is under the noise level, this experiment provides an upper bound estimate of protonated ^{13}C of 5% of the original signals for all the regions, from its noise level. We also attempted to obtain ^{13}C MAS spectra

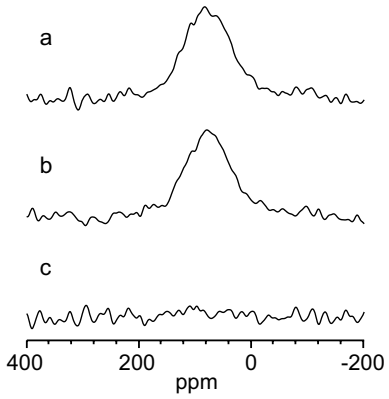

Fig. 5. ^{13}C MAS spectra of platelet graphite nanofibers (14.4 mg) (a) without and (b) with ^{13}C–^{1}H dipolar dephasing using ^{13}C–^{1}H REDOR, together with (c) the difference spectrum between (a) and (b). The signals were excited by a $\pi/2$-pulse. See Ref. [3] about the pulse sequence. The spectra were acquired at a spinning speed of 20,000 Hz ± 5.0 Hz without ^{1}H RF decoupling. Background signals were removed in (a,b) by subtracting the spectrum obtained without the sample using the corresponding pulse sequence. To minimize contribution of the residual background signals, recycle delays of 8 s were employed. No major spectral changes from Fig. 4 were observed in (a). The experimental time was 13.7 h for 6144 scans. Gaussian broadening of 10 ppm was applied to the spectra.

with polarization transfer from ^{1}H spins using the dipolar INEPT method [16], which allows for a quantitative signal analysis under fast spinning. However, the ^{13}C MAS spectrum acquired for the GNF sample exhibited no signals above the noise level after 5,120 scans with recycle delays of 3 s (data not shown). This is consistent with the result of our dipolar dephasing experiment. Hence, there is only, if any, a small fraction of protonated carbons in the GNF sample. Since we could not identify any protonated sp^3 carbons, it is likely that sp^2 carbons are the predominant species in this sample.

3.3. AFM observation and nanoindentation

A typical morphology of the platelet GNF observed by AFM is shown in Fig. 6. Nanoindentation has been performed on three individual GNFs using a special diamond-tipped cantilever with an included angle of about 60° and a tip radius less than 50 nm. Fracture of the GNF occurs during indentation. The images of the GNF before and after fracture are shown in Fig. 7(a) and (b), respectively. A cross sectional analysis (Fig. 7(c)) illustrates that the GNF has a trapezoidal shape. The cross sectional area of the GNF can be estimated by determining the geometrical parameters a, b, and l. The corresponding force displacement curve is also shown in Fig. 7(d). As can be seen, a clear step (AB in Fig. 7(d)) with a zig-zag characteristic occurs in the loading curve due to the fracture of the GNF. The energy released during the fracture, E_f, can be estimated by integrating the shaded area under the loading curve [17]. Note that the fracture energy measured here consists of the energy used for both crack initiation and propagation. The three GNFs loaded to fracture yield an average fracture energy of $3.85 \pm 0.95\ J/m^2$ (specifically, the values were 2.32, 3.65, and 5.58 J/m^2).

The fracture energy reported here is much higher than the cohesive energy values of graphite reported in the literature [18–26]. The theoretically calculated cohesive energy of neighboring graphene sheets in an ideal graphite crystal ranges from $0.048\ J/m^2$ to $1.028\ J/m^2$ [18–24] while the experimentally determined values are between $0.21\ J/m^2$ and $0.31\ J/m^2$ [24–26]. The cleavage energy of graphite is normally 18% higher than the cohesive energy [24]. The difference between the fracture energy values measured in this study and the cohesive energy values reported in the literature may be due to the fact that the cohesive energy is related to the reversible separation of neighboring layers in graphite while the fracture energy measured in this study is related to the irreversible fracture of these graphite platelet nanofiber structures. Since the diamond tip used in the fracture test has a tip radius of ~50 nm while the spacing between the finite graphene sheets is only about 0.34 nm, many graphene sheets are deformed by the tip during the fracture and it is most likely that the fracture has separated not only one pair of neighboring graphene sheets but several pairs, either partially or fully. Besides, there is also the possibility that some C–C bonds (which have a much higher energy than the van der Waals forces responsible for the interaction between graphene sheets) might have broken during the fracture, and that individual sheets are also being "crumpled" during the indentation. All of these factors may contribute to a higher value for the fracture energy; in short, for such a system the experimental configuration, namely the tip type and size, the size of the graphite platelet nanofiber, and the method used for the loading to failure, all play a role in the fit value of a 'fracture energy'. A modeling study of the indentation used here would be of interest as it might uncover some details that cannot be observed through our indentation experiment, such as the detailed configuration of the finite graphene sheets stacked next to each other, in the loaded region beneath the tip.

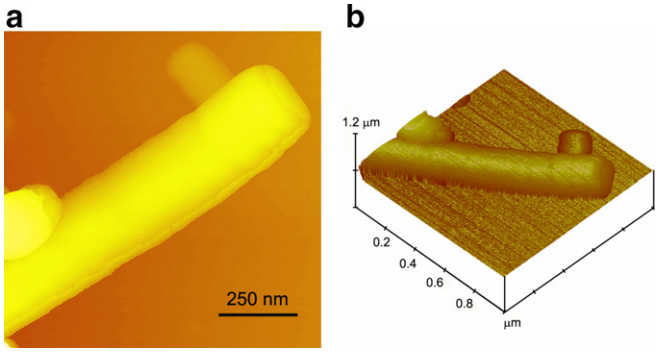

Fig. 6. An AFM image of a platelet graphite nanofiber: (a) two-dimensional; (b) three-dimensional.

To measure the hardness and elastic modulus of the GNFs, nanoindentation tests were also carried out with a Triboscope using a relatively blunt pyramidal Berkovich indenter with a tip radius of 100 nm to avoid the fracture of the GNFs so that the mechanical properties of 3 GNFs (different than those that were fractured) could be accurately determined. A typical indentation force (P)–displacement (h) curve is shown in Fig. 8. Hardness and reduced elastic modulus are calculated using the Oliver and Pharr method [27]. The hardness is given by

$$H = \frac{P_{max}}{A_c} \tag{1}$$

where P_{max} is the maximum indentation force and A_c is the projected contact area. The reduced elastic modulus is given by

$$E_r = \frac{\sqrt{\pi}}{2} \cdot \frac{S}{\sqrt{A_c}} \tag{2}$$

where S is the contact stiffness and E_r is the reduced modulus, which is related to the elastic modulus of sample E_s by

$$\frac{1}{E_r} = \frac{1 - \nu_i^2}{E_i} + \frac{1 - \nu_s^2}{E_s} \tag{3}$$

where E_i is the elastic modulus of the indenter, and ν_i and ν_s are Poisson's ratios of the indenter and the specimen. As shown in Fig. 7(c), the top surface of GNF is relatively flat with a width larger than 100 nm. The maximum nanoin-

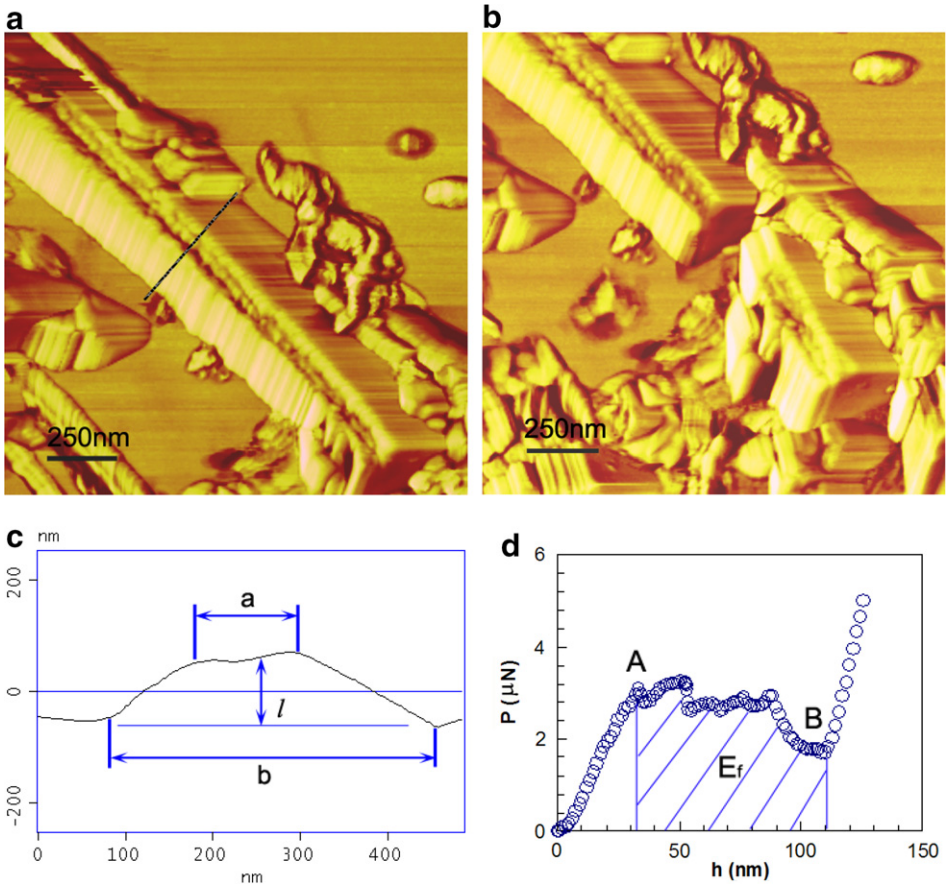

Fig. 7. Fracture of a platelet GNF by an AFM diamond tip. (a) GNF before fracture; (b) GNF after fracture; (c) A cross section view of the GNF, obtained from the line indicated in (a); (d) Corresponding force and displacement curve.

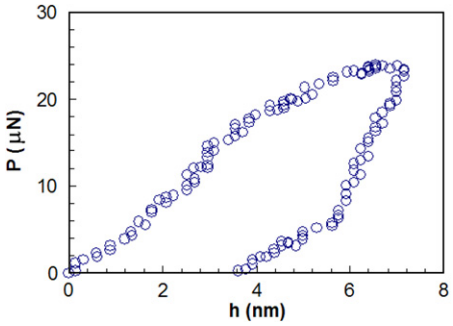

Fig. 8. A typical nanoindentation load–penetration depth curve on a platelet GNF.

dentation depth in this study is less than 10 nm, which creates an indent size much smaller than the dimension of the GNF. Therefore, the surface curvature effect is negligible. For the three GNFs tested, the average hardness was 1.2 ± 0.2 GPa (specifically, the values were 0.96, 1.22, and 1.46 GPa) and the average reduced modulus was 88 ± 23 GPa (specifically, 62.7, 78.6, and 123.2 GPa).

It should be noted that for an anisotropic material such as GNF, the hardness and modulus values calculated using the Oliver & Pharr method, which was developed based on an isotropic material, depend on the indentation direction and the orientation of the material. Vlassak and Nix [28] have shown that the formulae used for isotropic materials can be used for anisotropic materials, especially for those cases with higher symmetry. In the case of lower symmetry, they found that the indentation modulus depends on the shape of the indenter. A recent finite element analysis [29] has shown that the Oliver & Pharr method provides a first order approximation in the analysis of anisotropic mechanical properties of cortical bone, although the indentation modulus is influenced by the anisotropy. The measured hardness and modulus, given the highly anisotropic expected mechanical properties of such nanofibers based on their similarity to graphite, can be taken in the context of the above remarks. Moreover, a recent study of sample size effect on nanoindentation of micro-/nanostructures has also shown that the measured hardness and modulus by nanoindentation depend on both the sample size and its shape at small scales [5]. The GNFs studied in this research have a trapezoidal cross section (Fig. 7(c)) with an average "flat" top width of about 136 nm ($2R$) and an average height of 112 nm (h_0). This gives a radius to height ratio (R/h_0) of 0.6. Using the relationships developed in the literature [5] between the ratio of measured hardness/modulus to their true values and the sample shape ratio ($R/h_0 = 0.6$), the hardness and modulus measured in this study is a lower

bound estimate. The average contact depth of nanoindenation on the three GNFs is 6.9 nm, which gives a contact radius R_c of 36.4 nm assuming that the tip radius of Berkovich is 100 nm, and the average maximum penetration depth is 8.6 nm. This gives a value of $R_c/R = 0.54$ and a value of $h/h_0 = 0.077$. Using the relationships developed in the literature [5], the possible underestimation of hardness and modulus caused by the sample size effect in this study could be about 20% for hardness and 10% for modulus, respectively. Therefore, the average hardness value should be in the range from 1.2 ± 0.2 GPa to 1.5 ± 0.25 GPa and the average reduced elastic modulus from 88 ± 23 GPa to 97.7 ± 25.6 GPa.

4. Summary

We have studied a commercial sample of platelet graphite nanofibers. SEM and TEM data indicate that these fibers consist of stacked carbon (likely, graphene) sheets oriented perpendicular to the long axis of the fiber. Solid-state nuclear magnetic resonance data show that the fraction of hydrogenated carbon is under the detection limits (<5%) and that the nanofibers consist of primarily sp^2-bonded carbon. Mechanical measurements have been carried out on 3 different nanofibers by nanoindentation. The average hardness was in the range from 1.2 ± 0.2 GPa to 1.5 ± 0.25 GPa, the average reduced elastic modulus in the range from 88 ± 23 GPa to 97.7 ± 25.6 GPa, and the average fracture energy was 3.85 ± 0.95 J/m^2.

Acknowledgements

The authors would like to thank C. Jameson and J. Yesinowski for stimulating discussions, S. Li for help on SAED measurements, and L. Girifalco and W. Gerberich for their comments on the manuscript. Initial work on this project (XC and RSR) was supported from the NSF (DMR-0304508 and CMS-0304506) and by the NASA BIMat URETI # NCC-1-02037. The solid-state NMR work was supported in part by the Alzheimer's Association (NIRG 035123), the Dreyfus Foundation Teacher-Scholar Award program, and the NSF CAREER program (CHE 449952) for YI. Z.-H. Xu and X. Li were supported by the NSF (Grant No. EPS-0296165), the ACS Petroleum Research Fund (ACS PRF# 40450-AC10), the South Carolina Space Grant Consortium-NASA, and the University of South Carolina NanoCenter Seed Grant. The SEM, TEM, and XPS measurement were performed in the NU*ANCE* Center at Northwestern University. The NU*ANCE* Center is supported by the NSF-NSEC, NSF-MRSEC, Keck Foundation, the State of Illinois, and Northwestern University.

References

[1] Rodriguez NM, Chambers A, Baker RTK. Catalytic engineering of carbon nanostructures. Langmuir 1995;11(10):3862–6.

[2] Carneiro OC, Kim MS, Yim JB, Rodriguez NM, Baker RTK. Growth of graphite nanofibers from the iron-copper catalyzed decomposition of CO/H_2 mixtures. J Phys Chem B 2003;107(18):4237–44.

[3] Ishii Y, Wickramasinghe NP, Chimon S. A new approach in 1D and 2D C^{13} high-resolution solid-state NMR spectroscopy of paramagnetic organometallic complexes by very fast magic-angle spinning. J Am Chem Soc 2003;125(12):3438–9.

[4] Li XD, Bhushan B, Takashima K, Baek CW, Kim YK. Mechanical characterization of micro/nanoscale structures for MEMS/NEMS applications using nanoindentation techniques. Ultramicroscopy 2003;97(1–4):481–94.

[5] Xu ZH, Li XD. Sample size effect on nanoindentation of micro-/nanostructures. Acta Mater 2006;54(6):1699–703.

[6] Ton-That C, Shard AG, Teare DOH, Bradley RH. XPS and AFM surface studies of solvent-cast PS/PMMA blends. Polymer 2001;42(3):1121–9.

[7] Stankovich S, Piner RD, Chen X, Wu N, Nguyen ST, Ruoff RS. Stable aqueous dispersions of graphitic nanoplatelets via the reduction of exfoliated graphite oxide in the presence of poly(sodium 4-styrenesulfonate). J Mater Chem 2006;16(2):155–8.

[8] Lambert JB, Mazzola EP. Nuclear magnetic resonance spectroscopy. Upper Saddle River, New Jersy: Pearson Education Inc.; 2004.

[9] Resing HA, Hodgeman DKC, Baker JA, Poziomek EJ. C^{13} NMR-spectroscopy of the charcoal 4-vinylpyridine system. Carbon 1985;23(4):395–403.

[10] Hiroyama Y, Kume K. High-resolution C^{13} NMR-spectra in graphite chemical-shift and diamagnetism. Solid State Commun 1988;65(7):617–9.

[11] Goze-Bac C, Latil S, Lauginie P, Jourdain V, Conard J, Duclaux L, Rubio A, et al. Magnetic interactions in carbon nanostructures. Carbon 2002;40(10):1825–42.

[12] Freitas JCC, Emmerich FG, Cernicchiaro GRC, Sampaio LC, Bonagamba TJ. Magnetic susceptibility effects on C^{13} MAS NMR spectra of carbon materials and graphite. Solid State Nucl Magn Reson 2001;20(1–2):61–73.

[13] Pan HJ, Pruski M, Gerstein BC, Li F, Lannin JS. Local coordination of carbon-atoms in amorphous-carbon. Phys Rev B 1991;44(13):6741–5.

[14] Kaplan S, Jansen F, Machonkin M. Characterization of amorphous carbon–hydrogen films by solid-state nuclear magnetic-resonance. Appl Phys Lett 1985;47(7):750–3.

[15] Donnet C, Fontaine J, Lefebvre F, Grill A, Patel V, Jahnes C. Solid state C^{13} and H^1 nuclear magnetic resonance investigations of hydrogenated amorphous carbon. J Appl Phys 1999;85(6):3264–70.

[16] De Vita E, Frydman L. Spectral editing in C^{13} MAS NMR under moderately fast spinning conditions. J Magn Reson 2001;148(2):327–37.

[17] Li XD, Wang XN, Xiong QH, Eklund PC. Top-down structure and device fabrication using in situ nanomachining. Appl Phys Lett 2005;87(23):233113-1–3.

[18] Brennan RO. The interlayer binding in graphite. J Chem Phys 1952;20(1):40–8.

[19] Allinger NL. Conformational-analysis.130. mm2-hydrocarbon force field utilizing V1 and V2 torsional terms. J Am Chem Soc 1977;99(25):8127–34.

[20] Schabel MC, Martins JL. Energetics of interplanar binding in graphite. Phys Rev B 1992;46(1):7185–8.

[21] Trickey SB, Muller-Plathe F, Diercksen GHF, Boettger JC. Interplanar binding and lattice-relaxation in a graphite delayer. Phys Rev B 1992;45(8):4460–8.

[22] Charlier JC, Gonze X, Michenaud JP. Graphite interplanar bonding-electronic delocalization and Van-der-Waals interaction. Europhys Lett 1994;28(6):403–8.

[23] Rydberg H, Jacobson N, Hyldgaard P, Simak SI, Lundqvist BI, Langreth DC. Hard numbers on soft matter. Surf Sci 2003;532–535:606–10.

[24] Girifalco LA, Lad RA. Energy of cohesion, compressibility, and the potential energy functions of the graphite system. J Chem Phys 1956;25(4):693–7.
[25] Benedict LX, Chopra NG, Cohen ML, Zettl A, Louie SG, Crespi VH. Microscopic determination of the interlayer binding energy in graphite. Chem Phys Lett 1998;286(5–6):490–6.
[26] Zacharia R, Ulbricht H, Hertel T. Interlayer cohesive energy of graphite from thermal desorption of polyaromatic hydrocarbons. Phys Rev B 2004;69:155406-1–7.
[27] Oliver WC, Pharr GM. An improved technique for determining hardness and elastic-modulus using load and displacement sensing indentation experiments. J Mater Res 1992;7(6):1564–83.
[28] Vlassak JJ, Nix WD. Indentation modulus of elastically anisotropic half-spaces. Phil Mag A 1993;67(5):1045–56.
[29] Fan Z, Rho JY, Swadener JG. Three-dimensional finite element analysis of the effects of anisotropy on bone mechanical properties measured by nanoindentation. J Mater Res 2004;19(1):114–23.